

Entanglement transitions in quantum-enhanced experiments

Shane P. Kelly^{1, 2, *} and Jamir Marino²

¹*Mani L. Bhaumik Institute for Theoretical Physics, Department of Physics and Astronomy, University of California at Los Angeles, Los Angeles, CA 90095*

²*Institute for Physics, Johannes Gutenberg University of Mainz, D-55099 Mainz, Germany*

(Dated: June 10, 2024)

A quantum-enhanced experiment, in which information is transduced from a system of interest and processed on a quantum computer, has the possibility of exponential advantage in sampling tasks over a traditional experiment, where only the measurement outcomes of projective or weak measurements are stored on a classical computer. In this work, we demonstrate that, similar to the measurement induced phase transition (MIPT) occurring in traditional experiments, quantum-enhanced experiments can also show entanglement phase transitions. We introduce a noisy transduction operation which replaces projective measurements and acts independently on two qubits, recording the quantum state of one qubit in the measurement apparatus, while erasing the quantum state of the other qubit with the environment. We then construct a random brickwork circuit which shows an entanglement transition tuned by the rate of noisy transduction operations. Below the critical rate of noisy transduction, an extensive amount of entanglement is generated between regions of the system and apparatus, while above the critical rate, entanglement satisfies area law scaling. Our work delineates the prerequisites for quantum-enhanced experiments to manifest entanglement transitions, thereby establishing a foundational framework that connects quantum-enhanced sensing with emergent entanglement phenomena.

The transfer of information is a ubiquitous process in any experiment, technological development or daily interaction. Most of the time, these events involve simple conversion processes, and a direct analysis of channel capacities, or sampling of entropy, is no longer necessary in their design. Yet, as experiments become more elaborate, a direct analysis of channel capacity and information flow can become advantageous. This occurs in the classical realm, when machine learning is required to analyze large data sets [1], but it is also important in quantum experiments where sensing beyond the standard quantum limits [2–4] requires the observation of several quantum devices prepared in entangled states [5–8].

A key difference in the quantum domain is that quantum information can not be copied [9, 10]. Thus, the interrogation of a quantum system requires the transfer of information between the system and measurement apparatus, and necessarily results in disrupting the natural information dynamics of the system. This is sharply demonstrated by the measurement induced phase transition (MIPT) [11–14] that can occur in a unitary many body quantum system interrogated by a projective measurement process [15–55]. At a large measurement rate, the projective measurements disrupt information spreading, while below a critical threshold, quantum information spreads and generates strongly entangled states.

In this setting, classical information, in the form of projective measurement outcomes, is transferred to the measurement apparatus. More recently, the transfer of quantum information has been shown to achieve exponential advantage in sampling tasks compared to the transfer of classical information [56–58]. The advantage is gained in a quantum-enhanced experiment [56] where the measurement apparatus doesn't perform a projective measure-

ment, but instead transfers states to a quantum memory for post processing by a quantum computer. In this setting, the transfer of quantum information may seriously disrupt the natural dynamics of information in the system. This motivates us to investigate the possibility that the disruption results in a phase transition, similar to the MIPT.

Previous work [59] observed that the perfect transfer of quantum information does not result in an entanglement transition similar to the MIPT. In the MIPT, the transition occurs at a critical measurement rate, below which volume law entangled states are produced and above which area law entangled states are produced. Here, the entanglement is only observed in the pure states conditioned on the measurement outcomes. If the measurement outcomes are ignored, the system only shows a mixed unentangled state regardless of the measurement rate. In the previous work [59], projective measurements were replaced by a swap operation that transferred the complete qubit state to a measurement apparatus. While a different transition was observed, the entanglement transition was lost. Regardless of conditioning on the measurement apparatus, the late time system states were short ranged entangled mixed states. This investigation therefore suggests that quantum information transfer does not produce an entanglement transition in the way classical information transfer does.

In this Letter, and in the accompanying work [60], we reveal a more complete picture and demonstrate that entanglement transitions are indeed possible. In particular, we produce an interrogation procedure that transfers quantum information to an apparatus and shows an entanglement transition generalizing the MIPT. A key insight is that projective measurement of a qubit obtains

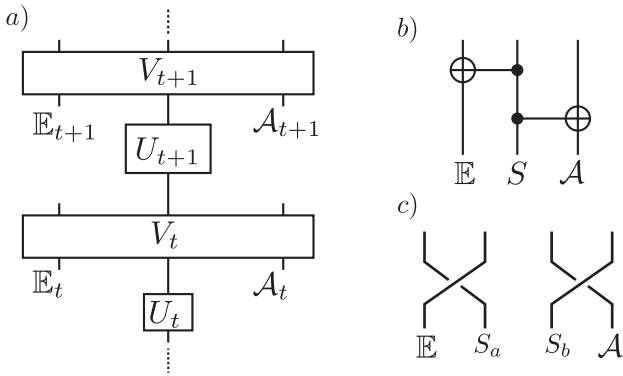


FIG. 1. Unitary dynamics of a system, S , being probed in a quantum-enhanced experiment. When the apparatus, \mathcal{A} , couples to the system, noise is generally introduced, and is modeled by a Markovian environment, \mathbb{E} , with T uncorrelated components \mathbb{E}_t for $t = 1 \dots T$. The unitary V_t , models the coupling operation which produces the signal in the t^{th} component of the apparatus \mathcal{A}_t , and injects noise due to the environment \mathbb{E}_t . b) Unitary implementation of a projective measurement on a single qubit. c) The noisy transduction operation acting on two qubits S_a and S_b .

logical information at the cost of destroying phase information, and that this symmetry between information gain and loss is spontaneously broken in the MIPT. We discuss the general implications of this “information exchange symmetry” in the accompanying work, and introduce in this Letter a “noisy transduction operation” that possesses this symmetry and transfers quantum information to a quantum apparatus.

Below we present an entanglement transition tuned by the rate of the noisy transduction operations. In contrast to projective measurements, an environment is explicitly introduced and it is no longer obvious the quantum conditional entropies considered in the MIPT remain entanglement quantifiers. Surprisingly, we find that in addition to guaranteeing the existence of a transition, the information exchange symmetry also guarantees the quantum conditional entropies are quantifiers of entanglement, such that the transition is again between area law and volume law entangled states. In contrast to the MIPT, noisy transduction transfers quantum information and allows for quantum advantage in the quantum post processing of that information on a quantum computer.

A framework for experiments: We begin by constructing a framework that can capture both experiments involving projective measurements and quantum-enhanced experiments involving the transduction of quantum information from system to a quantum apparatus. The framework considers any experiment that regularly probes the natural dynamics of a system of interest. The probe will be modeled by a coupling to an experimental apparatus. To capture the noise introduced by various probes, such as projective measurements, we will

allow for the couplings to interact with environment degrees of freedom. Finally to capture all sources of noise and signal on equal footing, we will consider an explicit purification [61] of the environment such that the full dynamics will be modeled by a sequence of unitaries coupling system, apparatus and environment.

Concretely, we will consider an experiment composed of T steps interacting with T independent components of a measurement apparatus. Each step begins by allowing the system to undergo its natural unitary dynamics $U(t)$, followed by a measurement process in which the system is coupled to the t^{th} component of the apparatus, \mathcal{A}_t . We allow this process to introduce Markovian noise by introducing an environment \mathbb{E} , also with T independent components which we label \mathbb{E}_t for $t = 1 \dots T$. The measurement process is described by a unitary $V(t)$ acting between the system, and the t^{th} components of the apparatus, and environment. The full dynamics of the system, environment and apparatus is shown in Fig 1, and is described by a unitary $\mathcal{U}_T = \prod_{t=1}^T V(t)U(t)$. In this Letter, we will assume the environment, system and apparatus are initialized in a pure state, $|\psi_{\mathbb{E}}\rangle \otimes |\psi_0\rangle \otimes |\psi_{\mathcal{A}}\rangle$ with no correlations between the T different components of the apparatus and environment. The T components of the environment and apparatus should be prepared with no correlations to ensure the T measurement processes are independent. We treat more general initial conditions in the Supplemental Material (SM).

While not immediately obvious, it has been known that such a unitary dynamics of system, apparatus and environment can model projective measurements [27, 61, 62]. The unitary implementing a projective measurement on a single qubit [27, 61] is shown in Fig. 1 b), where a controlled-not gate (CNOT) is applied between the measured system qubit and a qubit in the apparatus, followed by a second CNOT gate applied to the system qubit and a qubit in the environment. If the initial state of the system qubit was $|\psi\rangle = \psi_0|0\rangle + \psi_1|1\rangle$, and the initial state of the apparatus is $|0\rangle$, the mixed state on the system and apparatus after the two CNOTs will be $\rho = |\psi_0|^2|00\rangle\langle 00| + |\psi_1|^2|11\rangle\langle 11|$. Notice that this statistical distribution of quantum states involves the uncertainty of the measurement outcome, and is therefore not a pure state. Conditioning on one of the outcomes, say 0, in the apparatus, the conditional state in the system will be the pure state $|0\rangle$ obtained by applying the corresponding projector.

For the projective measurements, or equivalently the unitary implementation in Fig. 1 b), the final state in the apparatus is incoherent in the measurement basis since only classical information about the measurement basis has been transferred. For a general coupling unitary V_t , this need not be the case as V_t could potentially transfer a quantum state to the apparatus. Due to the potential advantage in sampling tasks, such experiments are considered as quantum enhanced [56]. As a concrete ex-

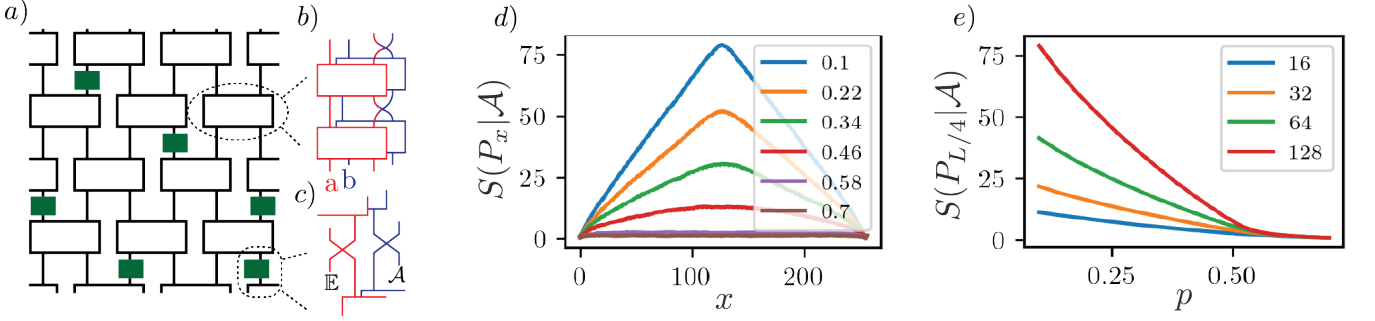


FIG. 2. a) Brickwork circuit showing an entanglement transition tuned by the rate of noisy transduction operations (shown in green). In panel a), the 'a' and 'b' qubits are grouped into one line. b) 4 two-qubit unitaries composing a brick. The unitaries acting on the 'a' qubits are shown in red, while those acting on the 'b' qubits are shown in blue. c) The noisy transduction operations swaps 'a' qubits into the environment, and 'b' qubits into the apparatus. Both apparatus and environment qubits are initialized in pure states. d) Volume law and area law scaling of quantum conditional entropy, $S(P_x|\mathcal{A})$ for a continuous subsystem composed of x sites, and conditioned on the state in the apparatus. Here, we consider a system of $L = 128$ sites; the legend gives the corresponding noisy transduction rate p . e) Quantum conditional entropy $S(P_x|\mathcal{A})$ for $x = L/4$ as a function of p ; the legend shows the number of sites L . A transition from volume law to area law scaling appears at $p = 0.52$. A careful scaling analysis is performed in the SM.

ample, we will consider the “noisy transduction” operation shown in Fig. 1 c) and that acts on two qubits of the system. The quantum state of the qubit S_b is transduced [63] into the apparatus by a swap with the initially pure apparatus qubit, while the quantum state of another qubit, S_a , is destroyed and swapped with a initially pure environment qubit. At the end of the dynamics, all qubits in the environment are discarded and all qubits in the apparatus are stored for quantum post processing.

This experimental framework captures both the MIPT, where the unitaries V_t are composed of the projective measurement unitaries, and also the following quantum-enhanced experiment exhibiting an entanglement transition. We consider a brickwork random circuit acting on L sites where $U(t)$ implements either the even or odd layers of the brickwork. While in the MIPT circuit, the sites contains a single qubit, and $V(t)$ implements the projective measurement with probability p on each qubit, our quantum-enhanced experiment contains two qubits per site, with labels 'a' and 'b', and $V(t)$ implements the noisy transduction operation with probability p on each qubit, see Fig. 2. Furthermore, we require the system unitary, U_t , to be symmetric under exchange of the 'a' and 'b' qubits. This is accomplished as follows. At each step, an identical unitary chosen from the Clifford group, or Haar measure, is applied to both the a and b qudits of two neighboring sites. The two sets of qubit a and b are then coupled by a swap operation occurring on the even sites, followed by another pair of identical two-qubit random unitaries. The full sequence of unitary and swaps comprising a brick is shown in Fig. 2 b). Finally, we note that the choice of a brickwork structure and random unitaries is simply for analytic and numerical

control of the problem. Similar to other random unitary approaches [11], the results are expected to hold for any chaotic unitary dynamics.

Noisy Transduction Induced Phase Transition: The resulting information dynamics of this brickwork quantum enhanced experiment shows similar phenomenology to the MIPT. The main difference is that instead of conditioning the state of the system on projective measurement outcomes, it is conditioned on the quantum state using the quantum conditional entropy. The quantum conditional entropy [64, 65], $S(A|B) = S(\rho_{AB}) - S(\rho_B)$, is defined using the von-Neumann entropy, $S(\rho) = -\text{tr}[\rho \ln \rho]$, on two subsystems A and B , where $\rho_A = \text{tr}_B[\rho_{AB}]$. For the quantum-enhanced experiments introduced in this Letter, we consider the von-Neumann entropies

$$S(P_S; M) = S(\text{tr}_{P_S^c \cup M^c} [|\psi_T\rangle \langle \psi_T|]) \quad (1)$$

for the reduced density matrix of $|\psi_T\rangle = \mathcal{U}_T |\psi_{\mathbb{E}}\rangle \otimes |\psi_0\rangle \otimes |\psi_{\mathcal{A}}\rangle$, on the subsystems $P_S \cup M$, where P_S is a subset of the system, and $M \subset \mathcal{A} \cup \mathbb{E}$ is a subset of the apparatus, \mathcal{A} , and environment, \mathbb{E} . We have taken the notation where P_S^c is the complement of P_S within the system such that $P_S \cup P_S^c = S$, and M^c is defined by $M^c \cup M = \mathbb{E} \cup \mathcal{A}$. We are then interested in the quantum conditional entropy $S(P_S|M) = S(P_S; M) - S(\emptyset; M)$, where \emptyset is the empty set and $S(\emptyset; M)$ is the von-Neumann entropy of the reduced state on M . In MIPT, the apparatus contains the measurement outcomes and $S(P_S|\mathcal{A})$ observes the entanglement transition [27]. Below the transition, $S(P_S|\mathcal{A})$, scales with the size of the region P_S and characterizes volume law entanglement, while above the critical measurement rate, $S(P_S|\mathcal{A})$ scales independently of the size of P_S , characterising area law entanglement.

In Fig. 2, we show results from the numerical simulation [66–68] of circuits in which the unitaries are chosen randomly from the two qubit Clifford group for system sizes up to $L = 256$. In Fig. 2 d), the entropy density in the chain, conditioned on the quantum state in the apparatus, $S(P_x|\mathcal{A})$ shows both area law, for $p < 0.514$, and volume law curves for $p > 0.514$. While, in Fig. 2 e), the quarter cut entropy as a function of p shows the transition between area law and volume law scaling.

In the SM, we also consider analogies of purification dynamics [69, 70], and use the tripartite mutual information [71], to identify the critical point at $p = 0.514$ and critical exponent of $\nu = 1.16$ distinct from the analogous exponent in MIPT ($\nu \approx 1.3$) [69, 71, 72]. This distinct universality is also observed in an analytic investigation of the transition [60], in the limit of a large local hilbert space, also finds a distinct universality class from the MIPT.

Entanglement structure: Since the state on the system and apparatus is mixed, the von-Neumann entropy is not an entanglement quantifier [73]. Nonetheless, the volume law scaling of the quantum conditional entropy does capture volume law scaling of entanglement. To demonstrate this, we first need to introduce the information exchange (IE) symmetry. In Ref [60], we show that this symmetry is required for an entanglement transition in a quantum enhanced experiments to generalize the phenomenology of the MIPT. Here, we introduce this symmetry and show how it constrains the entanglement structure of the mixed state on the system and apparatus.

The IE symmetry is the weakest form of three symmetries in which the symmetry transformation is exchange of apparatus and environment. While the transformation is the same for each symmetry, what is required to be symmetric is different. In the strongest version, which we call the Apparatus-Environment Exchange (AEE) symmetry, the full quantum state is required to be symmetric, see Fig. 3 a). Projective measurements satisfy this symmetry since the two CNOTs in Fig. 1 b) commute.

We found that exact state equivalence of the AEE symmetry is unnecessarily restrictive to guarantee an entanglement transition. Instead, it is sufficient to require symmetry under exchange of apparatus and environment up to a local unitary operation applied independently to the system sites, apparatus and environment, see Fig. 3 b). Since this requirement enforces equivalence up to the local unitaries, we consider it the Local Unitary Exchange (LUE) symmetry. While the AEE symmetry doesn't hold for the noisy transduction operation, the LUE symmetry does. For this operation the local unitary on the system is the exchange of the two system qubits a and b , while the local unitary on the apparatus and environment are the identity.

The LUE symmetry guarantees that the entropies sat-

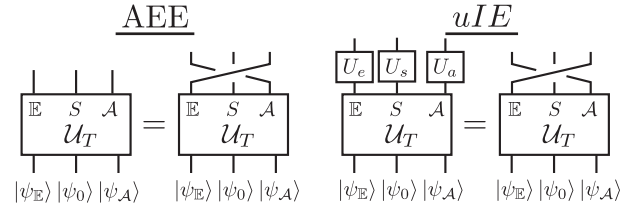


FIG. 3. Two symmetries a quantum enhanced experiment, $|\psi_T\rangle$, can posses. The apparatus-environment exchange symmetry (AEE) is shown on the left and requires the experiment be symmetric under exchange of apparatus and environment. While on the right, the Local Unitary Exchange symmetry (LUE) is shown. It also requires that the experiment be symmetric under exchange of apparatus and environment, but only up to some unitary transform, $U_e \otimes U_s \otimes U_a$, which is separable across environment, system and apparatus.

isfy,

$$S(P_S; \mathcal{A}) = S(P_S; \mathbb{E}), \quad (2)$$

which hold for any P_S . This implies that an observer of the apparatus and a fictitious observer of the environment have equivalent information about the system, $S(P_S|\mathcal{A}) = S(P_S|\mathbb{E})$. We designate any experiment that satisfies this relation for all P_S and times, T , as satisfying the IE symmetry. In contrast to the AEE symmetry which requires the state to be symmetric under exchange of apparatus and environment, the IE symmetry only requires symmetry of the entropies $S(P_S; \mathcal{A})$.

In combination with the global purity of total state, $|\psi_T\rangle$, on the system, apparatus and environment, the IE symmetry implies the quantum conditional entropies satisfy $S(P_S|\mathcal{A}) = S(P_S^c|\mathcal{A})$. This property is very natural for projective measurements, as the conditional state on the system is pure such that the entropy of a subsystem is equal to the entropy of its complement. Thus, in terms of the conditional entropies, the information exchange symmetry ensures the conditional state on the system behaves like a pure state.

Physically this ensures entanglement between regions P_S and $P_S^c \cup \mathcal{A}$. This is seen by using the IE symmetry to derive $S(P_x|\mathcal{A}) = -S(P_x|P_x^c \cup \mathcal{A})$ and the results of Refs [74, 75], which explain what it means to condition on a quantum state. In particular, they show a negative quantum conditional entropy of magnitude $|S(A|B)|$ implies the ability to distill $|S(A|B)|$ Bell pairs between the two regions. Thus, volume law scaling of $S(P_x|\mathcal{A})$ is equivalent to an extensive number of distillable Bell pairs between P_S and $P_S^c \cup \mathcal{A}$. Note that while the negative quantum conditional entropy gives the number of distillable Bell pairs, it is not an entanglement monotone because it can be both positive and negative and is not strictly zero for unentangled states.

The same symmetry and arguments hold for the entanglement phenomenon in the MIPT, except that the

state on the apparatus is diagonal in the measurement basis. The nature of classical measurements therefore forces all entanglement to be on the system (between P_x and P_x^c), while for a quantum enhanced experiment, the entanglement can also spreads onto the apparatus. Finally, subadditivity can be used to show [76], that the IE symmetry implies $S(P_x|\mathcal{A}) \geq 0$ which guarantees finite entanglement in both the area law and the volume law phase.

Discussion: In this work, we have demonstrated that the transfer of quantum information to a measurement apparatus can induce a phase transition in the dynamics of quantum information. This generalizes the MIPT, where the transfer of classical information induces the phase transition. We then identified the IE symmetry which controls the entanglement structure of such transitions. In both cases, the quantum conditional entropy $S(P_S|\mathcal{A})$ shows a transition from volume law scaling for small interrogation rates, to area law scaling for large interrogation rates. Of particular importance, the IE symmetry guarantees this quantum conditional entropy quantifies entanglement between regions P_S and $P_S^c \cup \mathcal{A}$. Furthermore, the entanglement transition is lost if the information in the apparatus is discarded. In both the experiments considered here and in the MIPT, the system quickly approaches a maximally mixed state when the information in the apparatus is discarded.

In Ref [60], we discuss the generality of entanglement transitions occurring in quantum enhanced experiments. In particular, we discuss gates chosen from the full Haar measure and construct a general replica theory for quantum enhanced experiments. We show how the LUE and IE symmetries can be used to guarantee and probe a minimal subgroup of the replica symmetry. When this minimal subgroup is spontaneously broken, the generalized form of the MIPT transition results. Finally, we showed how probe spontaneous breaking of the IE symmetry, and use it to describe the entanglement transition phenomenology without reference to replicas.

We expect exciting directions stemming from the observation that the IE symmetry is a symmetry between information quantifiers, and therefore suggests the symmetry applies generically to communication tasks. For example, the IE symmetry implies certain tasks which require decoding information about the system using the apparatus are equivalent to tasks which attempts to do so via the environment. One such task, related to dynamical purification [69], is the decoding the initial system state from the final system state and apparatus (or environment). In the SM [76], we show a symmetry breaking transition occurs in the capacity to perform this tasks (using either the apparatus or environment). It is interesting to wonder if this type of symmetry breaking might occur for other types of tasks, such as in thermodynamics or computation.

Acknowledgements: We greatly appreciate com-

ments on the first version of the manuscript by Zack Weinstein and Gerald E. Fux. We thank Martino Stefanini, Dominic Gribben, Oksana Chelpanova, and Riccardo Javier Valencia Tortora for valuable discussions on the information exchange symmetry. We are also grateful to Zack Weinstein and Ehud Altman for stimulating ideas. We acknowledge support by the Deutsche Forschungsgemeinschaft (DFG, German Research Foundation) – Project-ID 429529648 – TRR 306 QuCoLiMa (“Quantum Cooperativity of Light and Matter”), by the Dynamics and Topology Centre funded by the State of Rhineland Palatinate, and by the QuantERA II Programme that has received funding from the European Union’s Horizon 2020 research and innovation programme under Grant Agreement No 101017733 (‘QuSiED’) and by the DFG (project number 499037529). The authors gratefully acknowledge the computing time granted on the supercomputer MOGON 2 at Johannes Gutenberg-University Mainz (hpc.uni-mainz.de).

* skelly@physics.ucla.edu

- [1] D. J. C. MacKay, *Information Theory, Inference & Learning Algorithms* (Cambridge University Press, USA, 2002).
- [2] C. L. Degen, F. Reinhard, and P. Cappellaro, Quantum sensing, *Rev. Mod. Phys.* **89**, 035002 (2017).
- [3] G. Tóth and I. Apellaniz, Quantum metrology from a quantum information science perspective, *Journal of Physics A: Mathematical and Theoretical* **47**, 424006 (2014).
- [4] L. Pezzè, A. Smerzi, M. K. Oberthaler, R. Schmied, and P. Treutlein, Quantum metrology with nonclassical states of atomic ensembles, *Rev. Mod. Phys.* **90**, 035005 (2018).
- [5] F. Fröwis, P. Sekatski, W. Dür, N. Gisin, and N. Sangouard, Macroscopic quantum states: Measures, fragility, and implementations, *Rev. Mod. Phys.* **90**, 025004 (2018).
- [6] J. Franke, S. R. Muleady, R. Kaubruegger, F. Kranzl, R. Blatt, A. M. Rey, M. K. Joshi, and C. F. Roos, Quantum-enhanced sensing on optical transitions through finite-range interactions, *Nature* (2023).
- [7] K. A. Gilmore, M. Affolter, R. J. Lewis-Swan, D. Barberena, E. Jordan, A. M. Rey, and J. J. Bollinger, Quantum-enhanced sensing of displacements and electric fields with two-dimensional trapped-ion crystals, *Science* **373**, 673 (2021).
- [8] W. Muessel, H. Strobel, D. Linnemann, D. B. Hume, and M. K. Oberthaler, Scalable spin squeezing for quantum-enhanced magnetometry with bose-einstein condensates, *Phys. Rev. Lett.* **113**, 103004 (2014).
- [9] W. K. Wootters and W. H. Zurek, A single quantum cannot be cloned, *Nature* **299**, 802 (1982).
- [10] D. Dieks, Communication by EPR devices, *Physics Letters A* **92**, 271 (1982).
- [11] M. P. A. Fisher, V. Khemani, A. Nahum, and S. Vijay, *Random quantum circuits* (2022), [arxiv:2207.14280](https://arxiv.org/abs/2207.14280).
- [12] A. Chan, R. M. Nandkishore, M. Pretko, and G. Smith, Unitary-projective entanglement dynamics, *Phys. Rev. B*

99, 224307 (2019).

[13] B. Skinner, J. Ruhman, and A. Nahum, Measurement-induced phase transitions in the dynamics of entanglement, *Phys. Rev. X* **9**, 031009 (2019).

[14] Y. Li, X. Chen, and M. P. A. Fisher, Quantum zeno effect and the many-body entanglement transition, *Phys. Rev. B* **98** (2018).

[15] A. Nahum, S. Roy, B. Skinner, and J. Ruhman, Measurement and entanglement phase transitions in all-to-all quantum circuits, on quantum trees, and in landau-ginsburg theory, *PRX Quantum* **2**, 010352 (2021).

[16] X. Turkeshi, R. Fazio, and M. Dalmonte, Measurement-induced criticality in (2+1)-dimensional hybrid quantum circuits, *Phys. Rev. B* **102**, 014315 (2020).

[17] A. Lavasani, Y. Alavirad, and M. Barkeshli, Measurement-induced topological entanglement transitions in symmetric random quantum circuits, *Nature Physics* **17**, 342 (2021).

[18] S. Sang and T. H. Hsieh, Measurement-protected quantum phases, *Phys. Rev. Research* **3**, 023200 (2021).

[19] A. Lavasani, Y. Alavirad, and M. Barkeshli, Topological order and criticality in (2+1)D monitored random quantum circuits, *Phys. Rev. Lett.* **127**, 235701 (2021).

[20] S. Sharma, X. Turkeshi, R. Fazio, and M. Dalmonte, Measurement-induced criticality in extended and long-range unitary circuits, *SciPost Phys. Core* **5**, 023 (2022).

[21] O. Lunt, M. Szniszewski, and A. Pal, Measurement-induced criticality and entanglement clusters: A study of one-dimensional and two-dimensional clifford circuits, *Phys. Rev. B* **104**, 155111 (2021).

[22] Y. Bao, S. Choi, and E. Altman, Symmetry enriched phases of quantum circuits, *Annals of Physics* **435**, 168618 (2021).

[23] Z. Weinstein, Y. Bao, and E. Altman, Measurement-induced power-law negativity in an open monitored quantum circuit, *Phys. Rev. Lett.* **129**, 080501 (2022).

[24] O. Alberton, M. Buchhold, and S. Diehl, Entanglement transition in a monitored free-fermion chain: From extended criticality to area law, *Phys. Rev. Lett.* **126**, 170602 (2021).

[25] M. Buchhold, Y. Minoguchi, A. Altland, and S. Diehl, Effective theory for the measurement-induced phase transition of dirac fermions, *Phys. Rev. X* **11**, 041004 (2021).

[26] T. Müller, S. Diehl, and M. Buchhold, Measurement-induced dark state phase transitions in long-ranged fermion systems, *Phys. Rev. Lett.* **128**, 010605 (2022).

[27] Y. Bao, S. Choi, and E. Altman, Theory of the phase transition in random unitary circuits with measurements, *Phys. Rev. B* **101**, 104301 (2020).

[28] C.-M. Jian, Y.-Z. You, R. Vasseur, and A. W. W. Ludwig, Measurement-induced criticality in random quantum circuits, *Phys. Rev. B* **101**, 104302 (2020).

[29] G. Piccitto, A. Russomanno, and D. Rossini, Entanglement transitions in the quantum ising chain: A comparison between different unravelings of the same lindbladian, *Phys. Rev. B* **105**, 064305 (2022).

[30] P. Sierant, G. Chiriacò, F. M. Surace, S. Sharma, X. Turkeshi, M. Dalmonte, R. Fazio, and G. Pagano, Dissipative Floquet Dynamics: from Steady State to Measurement Induced Criticality in Trapped-ion Chains, *Quantum* **6**, 638 (2022).

[31] S. Murciano, P. Calabrese, and L. Piroli, Symmetry-resolved page curves, *Phys. Rev. D* **106**, 046015 (2022).

[32] S.-K. Jian, C. Liu, X. Chen, B. Swingle, and P. Zhang, Measurement-induced phase transition in the monitored sachdev-ye-kitaev model, *Phys. Rev. Lett.* **127**, 140601 (2021).

[33] P. Sierant, M. Schirò, M. Lewenstein, and X. Turkeshi, Measurement-induced phase transitions in $(d+1)$ -dimensional stabilizer circuits, *Phys. Rev. B* **106**, 214316 (2022).

[34] Y. Li, Y. Zou, P. Glorioso, E. Altman, and M. P. A. Fisher, Cross entropy benchmark for measurement-induced phase transitions, *Phys. Rev. Lett.* **130**, 220404 (2023).

[35] A. Pizzi, D. Malz, A. Nunnenkamp, and J. Knolle, Bridging the gap between classical and quantum many-body information dynamics, *Phys. Rev. B* **106**, 214303 (2022).

[36] P. Sierant and X. Turkeshi, Controlling entanglement at absorbing state phase transitions in random circuits, *Phys. Rev. Lett.* **130**, 120402 (2023).

[37] K. Yamamoto and R. Hamazaki, Localization properties in disordered quantum many-body dynamics under continuous measurement, *Phys. Rev. B* **107**, L220201 (2023).

[38] G. Chiriacò, M. Tsitsishvili, D. Poletti, R. Fazio, and M. Dalmonte, Diagrammatic method for many-body non-markovian dynamics: Memory effects and entanglement transitions, *Phys. Rev. B* **108**, 075151 (2023).

[39] S. Sudevan, D. Azses, E. G. Dalla Torre, E. Sela, and S. Das, Multipartite entanglement and quantum error identification in d -dimensional cluster states, *Phys. Rev. A* **108**, 022426 (2023).

[40] A. A. Akhtar, H.-Y. Hu, and Y.-Z. You, Measurement-induced criticality is tomographically optimal (2023), [arXiv:2308.01653 \[quant-ph\]](https://arxiv.org/abs/2308.01653).

[41] H. Lóio, A. De Luca, J. De Nardis, and X. Turkeshi, Purification timescales in monitored fermions, *Phys. Rev. B* **108**, L020306 (2023).

[42] E. V. H. Doggen, Y. Gefen, I. V. Gornyi, A. D. Mirlin, and D. G. Polyakov, Evolution of many-body systems under ancilla quantum measurements, *Phys. Rev. B* **107**, 214203 (2023).

[43] L. Viotti, A. L. Gramajo, P. I. Villar, F. C. Lombardo, and R. Fazio, Geometric phases along quantum trajectories, *Quantum* **7**, 1029 (2023).

[44] M. Tikhanovskaya, A. Lavasani, M. P. A. Fisher, and S. Vijay, Universality of the cross entropy in \mathbb{Z}_2 symmetric monitored quantum circuits (2023), [arXiv:2306.00058 \[quant-ph\]](https://arxiv.org/abs/2306.00058).

[45] S. Murciano, P. Sala, Y. Liu, R. S. K. Mong, and J. Alicea, Measurement-altered ising quantum criticality (2023), [arXiv:2302.04325 \[cond-mat.stat-mech\]](https://arxiv.org/abs/2302.04325).

[46] H. Wang, C. Liu, P. Zhang, and A. M. García-García, Entanglement transition and replica wormhole in the dissipative sachdev-ye-kitaev model (2023), [arXiv:2306.12571 \[quant-ph\]](https://arxiv.org/abs/2306.12571).

[47] I. Pohoiko, I. V. Gornyi, and A. D. Mirlin, Measurement-induced phase transition for free fermions above one dimension (2023), [arXiv:2309.12405 \[quant-ph\]](https://arxiv.org/abs/2309.12405).

[48] I. Pohoiko, P. Pöpperl, I. V. Gornyi, and A. D. Mirlin, Theory of free fermions under random projective measurements (2023), [arXiv:2304.03138 \[quant-ph\]](https://arxiv.org/abs/2304.03138).

[49] X. Cao, A. Tilloy, and A. D. Luca, Entanglement in a fermion chain under continuous monitoring, *SciPost Phys.* **7**, 024 (2019).

[50] M. Van Regemortel, Z.-P. Cian, A. Seif, H. Dehghani, and M. Hafezi, Entanglement entropy scaling transition under competing monitoring protocols, *Phys. Rev. Lett.*

126, 123604 (2021).

[51] A. Biella and M. Schiró, Many-Body Quantum Zeno Effect and Measurement-Induced Subradiance Transition, *Quantum* **5**, 528 (2021).

[52] X. Turkeshi, A. Biella, R. Fazio, M. Dalmonte, and M. Schiró, Measurement-induced entanglement transitions in the quantum ising chain: From infinite to zero clicks, *Phys. Rev. B* **103**, 224210 (2021).

[53] X. Turkeshi, M. Dalmonte, R. Fazio, and M. Schirò, Entanglement transitions from stochastic resetting of non-hermitian quasiparticles, *Phys. Rev. B* **105**, L241114 (2022).

[54] S. Liu, M.-R. Li, S.-X. Zhang, and S.-K. Jian, Entanglement structure and information protection in noisy hybrid quantum circuits (2024), [arXiv:2401.01593 \[quant-ph\]](https://arxiv.org/abs/2401.01593).

[55] S. Liu, M.-R. Li, S.-X. Zhang, S.-K. Jian, and H. Yao, Noise-induced phase transitions in hybrid quantum circuits (2024), [arXiv:2401.16631 \[quant-ph\]](https://arxiv.org/abs/2401.16631).

[56] H.-Y. Huang, M. Broughton, J. Cotler, S. Chen, J. Li, M. Mohseni, H. Neven, R. Babbush, R. Kueng, J. Preskill, and J. R. McClean, Quantum advantage in learning from experiments, *Science* **376**, 1182 (2022).

[57] H.-Y. Huang, R. Kueng, and J. Preskill, Information-theoretic bounds on quantum advantage in machine learning, *Phys. Rev. Lett.* **126**, 190505 (2021).

[58] D. Aharonov, J. Cotler, and X.-L. Qi, Quantum algorithmic measurement, *Nature communications* **13**, 887 (2022).

[59] Z. Weinstein, S. P. Kelly, J. Marino, and E. Altman, Scrambling transition in a radiative random unitary circuit, [arXiv preprint arXiv:2210.14242](https://arxiv.org/abs/2210.14242) (2022).

[60] S. P. Kelly and J. Marino, Generalizing measurement-induced phase transitions to information exchange symmetry breaking (2024), [arXiv:2402.***** \[quant-ph\]](https://arxiv.org/abs/2402.*****).

[61] M. A. Nielsen and I. L. Chuang, *Quantum computation and quantum information* (Cambridge university press, 2010).

[62] W. H. Zurek, Decoherence, einselection, and the quantum origins of the classical, *Rev. Mod. Phys.* **75**, 715 (2003).

[63] N. Lauk, N. Sinclair, S. Barzanjeh, J. P. Covey, M. Saffman, M. Spiropulu, and C. Simon, Perspectives on quantum transduction, *Quantum Science and Technology* **5**, 020501 (2020).

[64] N. J. Cerf and C. Adami, Negative entropy and information in quantum mechanics, *Phys. Rev. Lett.* **79**, 5194 (1997).

[65] N. J. Cerf and C. Adami, Quantum extension of conditional probability, *Phys. Rev. A* **60**, 893 (1999).

[66] D. Gottesman, Stabilizer Codes and Quantum Error Correction, [arXiv:quant-ph/9705052](https://arxiv.org/abs/quant-ph/9705052) (1997).

[67] D. Gottesman, The Heisenberg Representation of Quantum Computers, [arXiv:quant-ph/9807006](https://arxiv.org/abs/quant-ph/9807006) (1998).

[68] S. Aaronson and D. Gottesman, Improved simulation of stabilizer circuits, *Physical Review A* **70**, 052328 (2004).

[69] M. J. Gullans and D. A. Huse, Dynamical purification phase transition induced by quantum measurements, *Phys. Rev. X* **10**, 041020 (2020).

[70] S. Choi, Y. Bao, X.-L. Qi, and E. Altman, Quantum error correction in scrambling dynamics and measurement-induced phase transition, *Phys. Rev. Lett.* **125**, 030505 (2020).

[71] A. Zabalo, M. J. Gullans, J. H. Wilson, S. Gopalakrishnan, D. A. Huse, and J. H. Pixley, Critical properties of the measurement-induced transition in random quantum circuits, *Phys. Rev. B* **101**, 060301 (2020).

[72] Y. Li, X. Chen, and M. P. A. Fisher, Measurement-driven entanglement transition in hybrid quantum circuits, *Phys. Rev. B* **100**, 134306 (2019).

[73] R. Horodecki, P. Horodecki, M. Horodecki, and K. Horodecki, Quantum entanglement, *Rev. Mod. Phys.* **81**, 865 (2009).

[74] M. Horodecki, J. Oppenheim, and A. Winter, Partial quantum information, *Nature* **436**, 673 (2005).

[75] M. Horodecki, J. Oppenheim, and A. Winter, Quantum State Merging and Negative Information, *Commun. Math. Phys.* **269**, 107 (2007).

[76] See supplementary online material for details.

Supplemental material for: Entanglement transitions in quantum-enhanced experiments

Shane P. Kelly^{1,2,*} and Jamir Marino²

¹*Mani L. Bhaumik Institute for Theoretical Physics, Department of Physics and Astronomy, University of California at Los Angeles, Los Angeles, CA 90095*

²*Institute for Physics, Johannes Gutenberg University of Mainz, D-55099 Mainz, Germany*

(Dated: June 10, 2024)

CONTENTS

| | |
|---|---|
| I. Framework for considering temporal correlations | 1 |
| II. Entanglement properties of IE symmetric experiments | 2 |
| III. Critical exponents of the brickwork quantum enhanced circuit | 2 |
| IV. Dynamical purification and quantum communication transitions | 3 |
| V. Efficient simulation | 4 |
| A. Review of stabilizer states | 4 |
| B. The efficient algorithm | 5 |
| References | 6 |

I. FRAMEWORK FOR CONSIDERING TEMPORAL CORRELATIONS

In the main text we introduced the brickwork quantum circuit shown Fig. 1 which is a unitary circuit, \mathcal{U}_T that couples system, apparatus and environment. We considered the system, apparatus and environment to be in an initial pure state $|\psi_{T=0}\rangle = |\psi_{\mathbb{E}}\rangle \otimes |\psi_0\rangle \otimes |\psi_{\mathcal{A}}\rangle$ and discussed the spacial correlations of the late time state $|\psi_T\rangle = \mathcal{U}_T |\psi_{T=0}\rangle$, for $T = 4L$ layers of the brickwork circuit. In particular, we quantified the spacial correlations via the von-Neumann entropies

$$S(P_S; M) = S(\text{tr}_{P_S^c \cup M^c} [|\psi_T\rangle \langle \psi_T|]) \quad (1)$$

for the reduced density matrix of $|\psi_T\rangle$, on the subsystems $P_S \cup M$, where P_S is a subset of the system, and $M \subset \mathcal{A} \cup \mathbb{E}$ is a subset of the apparatus, \mathcal{A} , and environment, \mathbb{E} .

As mentioned in the main text the entanglement transition also manifests in the temporal correlations between the initial state and final state. To capture these correlations we initialize the system S in a maximally entangled state, $|\text{Bell}(S, S')\rangle$, with an auxiliary copy of the system S' . Both S and S' contain $2L$ qubits respectively. As the system S evolves and couples to the environment and apparatus under \mathcal{U}_T , the auxiliary system S' remains unchanged and acts as a reference for the initial state of S' . The final evolved state is

$$|\tilde{\psi}_T\rangle = \mathcal{U}_T |\psi_{\mathbb{E}}\rangle \otimes |\text{Bell}(S, S')\rangle \otimes |\psi_{\mathcal{A}}\rangle, \quad (2)$$

and we will consider the von-Neumann entropies

$$S(P_S, P'_S; M) = S(\text{tr}_{P_S^c \cup P'_S^c \cup M^c} [|\tilde{\psi}_T\rangle \langle \tilde{\psi}_T|]) \quad (3)$$

to capture temporal correlations between the initial and final state. Notice that by discarding the auxiliary qubits S' , the initial state becomes a maximally mixed state. In this scenario, $S(P_S, \emptyset; M)$ captures the late time correlations. For clarity, we will use the symbol $S_{\psi}(P_S; M)$ for the scenario in which the initial state of the system is in a pure state $|\psi_0\rangle$.

* skelly@physics.ucla.edu

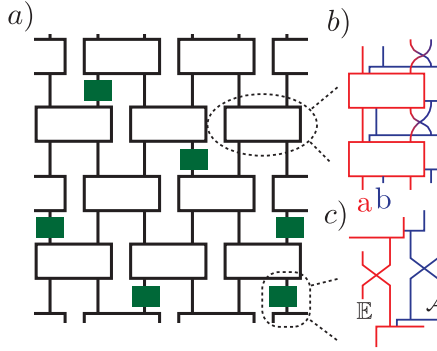


FIG. 1. Brickwork circuit composed of two qudit unitaries and probabilistic noisy transduction operations introduced in the main text.

II. ENTANGLEMENT PROPERTIES OF IE SYMMETRIC EXPERIMENTS

The IE symmetry guarantees a few important properties of the conditional entropies which relate $S(P_S|\mathcal{A})$ and $S(P_S, P'_S|\mathcal{A})$ to a quantification of entanglement. The first property is the complement symmetry,

$$S(P_S, P'_S; \mathcal{A}) = S(P_S^c, P_{S'}^c; \mathcal{A}), \quad (4)$$

which follows from the IE symmetry and the purity of the global state $|\mathcal{U}\rangle$.

The second property is due to sub-additivity applied to the environment, apparatus and the system:

$$S(\emptyset, \emptyset; \mathcal{A}) + S(\emptyset, \emptyset; \mathbb{E}) \leq S(P_S, P'_S; \mathcal{A}) + S(P_S, P'_S; \mathbb{E}) \quad (5)$$

which in combination with the IE symmetry yields the positivity of the quantum conditional entropy

$$S(P_S, P'_S|\mathcal{A}) \geq 0. \quad (6)$$

The same arguments hold for $S(P_S|M)$ such that $S(P_S|\mathcal{A}) \geq 0$

Finally, by using the IE symmetry and complement symmetry we can obtain

$$S(P_S, P'_S|\mathcal{A}) = -S(P_S \cup P'_S|\mathcal{A} \cup P_S^c \cup P_{S'}^c)$$

which implies in the volume law phase, the quantum conditional entropy $S(P_S \cup P'_S|\mathcal{A} \cup P_S^c \cup P_{S'}^c)$ is negative and scaling with volume. As discussed in the main text, negativity of quantum conditional entropy implies entanglement between the regions $P_S \cup P'_S$ and $P_S^c \cup P_{S'}^c \cup \mathcal{A}$. In the projective measurement dynamics, the state in the apparatus is classical, thus the entanglement is simply between the system regions as expected.

III. CRITICAL EXPONENTS OF THE BRICKWORK QUANTUM ENHANCED CIRCUIT

We now present the coherent information, and entanglement dynamics of the brickwork circuit where the two qubit unitaries are chosen from the Clifford group. Instead of performing complex algorithms [1] to uniformly sample the Clifford group we sample the two qudit unitaries in the following way. First, we uniformly apply one of the six single qubit Clifford unitaries to each of the two qubits with equal probability. Then, with a probability 0.9 we apply a CNOT followed again by two random single qubit unitary applied to each qubit. With probability 0.1, we only apply the random single qubit unitaries. While this procedure doesn't sample all possible two qubit Clifford gates, we believe it is sufficiently generic to capture the universal features of the entanglement transition.

In the main text, we showed evidence that this circuit shows a IE symmetry breaking phase transition by considering the final state quantum conditional entropy $S_\psi(P_x|\mathcal{A})$, where P_x included the a and b qubits from site 1 to x . To determine the critical point, we consider the tripartite mutual information, which was most successful in identify critical exponents for the measurement induced phase transition (MIPT) [2]. In a system with periodic boundary conditions, which is translationally invariant after disorder averaging, the tripartite mutual information, conditioned on the apparatus is constructed as

$$I_3 = 4S_\psi(R_1|\mathcal{A}) - 2S_\psi(R_1 \cup R_2|\mathcal{A}) - S_\psi(R_1 \cup R_3|\mathcal{A}) \quad (7)$$

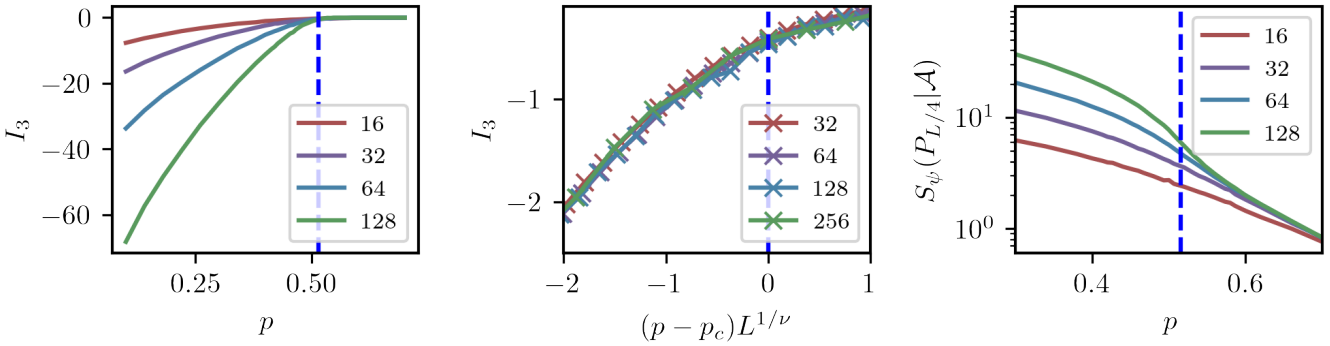


FIG. 2. Information exchange symmetry breaking after $T = 4L$ layers of the brickwork, for the system initialized in a pure product state. The number of sites, L , is shown in the legend of each figure and the critical probability $p_c = 0.514(2)$ is shown by a blue dashed vertical line. a) Conditional tripartite mutual information defined in Eq. 7 v.s. p . b) scaling collapse of tripartite mutual information for $\nu = 1.19(3)$; c) Quarter cut quantum conditional entropy $S_\psi(P_{L/4}|\mathcal{A})$ showing logarithmic scaling close to $p = p_c$.

where R_n contains the qubits at sites between $(n-1)L/4$ to $nL/4$. It is useful for identifying critical properties because of how it scales when the quantum conditional entropies $S_\psi(P_x|\mathcal{A})$ scale either linearly, logarithmic or independent of x . Above the critical noisy transduction rate, $S_\psi(P_x|\mathcal{A})$ obeys an area law (independent of x) and the conditional tripartite information vanishes $I_3 = 0$. While below the critical noisy transduction rate, $S_\psi(P_x|\mathcal{A})$ scales linearly with x such that I_3 is negative and scales linearly with system size. The conditional tripartite mutual information is particularly useful if at the critical point when $S_\psi(P_x|\mathcal{A})$ scales logarithmically in x . In this case, a direct analysis of $S_\psi(P_x|\mathcal{A})$ is difficult owing to a difficulty in distinguishing logarithmic from small power law scaling. Instead, the conditional tripartite mutual information is a universal constant when $S_\psi(P_x|\mathcal{A})$ scales logarithmic.

In Fig. 2, we see that the tripartite mutual information shows all three behaviors. Below the critical noisy transduction probability $p < p_c$, we find I_3 is negative and scaling with system size. Above criticality $p > p_c$ we find $I_3 \rightarrow 0$, and at criticality we find it is equal to a constant $I_3 = -0.5$ independent of system size. This suggests logarithmic scaling of $S_\psi(P_x|\mathcal{A})$, which we confirm qualitatively in Fig. 2 c). Since I_3 is constant at the critical point, identifying the critical point $p_c = 0.514(2)$ is straight forward. Furthermore, we find scaling collapse when rescaling probability around the critical point by $(p - p_c)L^{1/\nu}$, where $\nu = 1.19(3)$.

IV. DYNAMICAL PURIFICATION AND QUANTUM COMMUNICATION TRANSITIONS

In the MIPT, it was recognized early on that the entanglement transition can be viewed as a dynamical purification transition [3], or a transition in quantum coding [4–7]. Similarly, we show in Ref.[?] that the information exchange symmetry guarantees a similar transition in the quantum channel capacity of the channel between the initial system state and the finial state of the system and apparatus. This channel capacity is given by the coherent information

$$C(S' > S \cup \mathcal{A}) = S(S, \emptyset; \mathcal{A}) - S(S, S'; \mathcal{A}) \quad (8)$$

which gives the maximum number of qubits of information encoded in the initial state, S' , that can be recovered from the finial state of the system and apparatus $S \cup \mathcal{A}$. Numerical Clifford simulations of this quantity are shown in Fig. 3, and show a transition at the same critical point $p = 0.514$ and with the same exponent ν as for the quantum conditional entropy discussed above.

In the MIPT, the channel capacity (the coherent information) between S' and $S \cup \mathcal{A}$ was related to the purification dynamics of an initially maximally mixed system. A similar relation holds in general, and follows from the IE symmetry $S(S, S'; \mathcal{A}) = S(\emptyset, \emptyset; \mathcal{A})$ such that

$$C(S' > S \cup \mathcal{A}) = S(S, \emptyset; \mathcal{A}) - S(S, S'; \mathcal{A}) = S(S, \emptyset; \mathcal{A}) - S(\emptyset, \emptyset; \mathcal{A}) = S(S, \emptyset; \mathcal{A}) \quad (9)$$

Thus, phase transitions can be observed by monitoring the dynamics of the evolving quantum conditional entropy, $S(S, \emptyset; \mathcal{A})$, and evolving coherent information $C(S' > S \cup \mathcal{A})$. This also guarantees by subadditivity that $C(S' > S \cup \mathcal{A}) = S(S, \emptyset; \mathcal{A}) \geq 0$.

Finally the IE symmetry guarantees the channel between initial system S' to finial system S and environment \mathbb{E} shows the same transition, $C(S' > S \cup \mathcal{A}) = C(S' > S \cup \mathbb{E})$. Thus the IE symmetry guarantees a symmetry between

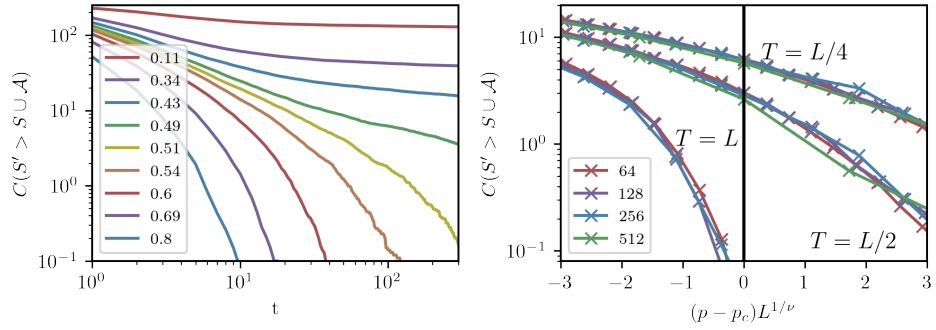


FIG. 3. Information exchange symmetry breaking shown by the quantum channel capacity between the initial state of the system, and the final state of both the system and apparatus. The channel capacity is quantified by the coherent information $C(S' > S \cup A)$. a) Coherent information v.s. time for a set of noisy transduction rates shown in the legend. In this figure, the system size is $L = 128$. b) Scaling collapse for the coherent information close to the critical noisy transduction rate p_c . The legend gives the system size L . No fitting was preformed here. Instead, the critical parameters $p_c = 0.514$ and $\nu = 1.19$ used are the optimal values obtained for the conditional tripartite mutual information I_3 . Finally, we note that the number of random samples considered ranged from 32, for $L = 512$, to 24000 for $L = 64$. The number of samples for $L = 512$ is extremely limited owing to each site containing 2 qubits such that the simulations are preformed on 1028 qubits.

two tasks: when decoding using the apparatus is possible, it is also possible with the environment. In Ref. ??, we argue this transition can be viewed as a spontaneous symmetry breaking of this task symmetry.

V. EFFICIENT SIMULATION

To simulate the expectation value of any observable on both system and apparatus the numerical simulation would require keeping track of $N = O(L^2)$ qubits because each time step introduces $O(L)$ apparatus qubits and the simulation evolves for $O(L)$ time steps. For stabilizer states, the memory requirement to represent the state scales as $O(N^2)$, such that simulating $O(L^2)$ qubits requires $O(L^4)$ memory and is not currently feasible for the system size we considered.

A. Review of stabilizer states

To circumvent this complexity we make use of the structure of stabilizer states to compute $S(P_S, P'_S; \mathcal{A})$ with only $O(L^2)$ memory complexity. A stabilizer state on N qubits has the form

$$\rho = \prod_{i=1}^M \frac{(1+g_i)}{2} \quad (10)$$

where g_i is a set of N commuting operators of the form

$$g_i = \gamma_i \prod_{x=1}^N X_i^{\alpha_{i,x}} z_i^{\beta_{i,x}} \quad (11)$$

where X_i and Z_i are Pauli operators, and the vectors $\vec{\alpha}_i$ and $\vec{\beta}_i$ are 2 vectors with components $\alpha_{i,x} \in \{0, 1\}$. Up to the phase $\gamma_i \in \{1, -1, i, -i\}$, the operators g_i are equivalent to a vector $\vec{v}_i = \vec{\alpha}_i \oplus \vec{\beta}_i$ living in the $2N$ dimensional vector space with discrete field \mathcal{F}_2 (addition and multiplication defined module 2). The operators g_i generate the commuting stabilizer group under operator multiplication. The representation of g_i in the $2N$ dimension vector space defines an isomorphism between the stabilizer group and a M dimensional subspace, where the stabilizer group multiplication maps to vector addition. A stabilizer state is then equivalently represented by either a group presentation of the stabilizer group, or by M linear independent vectors which span the M dimensional subspace. The second is used in numerical simulations, and in worse case a pure state requires $M = N$ vectors in a $2N$ dimensional vectors require memory scaling as $O(N^2)$.

The von-Neumann entropy of a stabilizer state is $S(\rho) = N - M$, and to compute, $S(P_S, P'_S; \mathcal{A})$, we simply need to identify the number of generators for the stabilizer group of the reduced state on the subsystem $P_S \cup P'_S \cup \mathcal{A}$.

The inefficient algorithm accomplishes this by tracking the evolution of the full stabilizer state on $S \cup S' \cup \mathcal{A}$, and computing the reduced state on $P_S \cup P'_S \cup \mathcal{A}$ when needed. Before introducing the efficient algorithm, we review the necessary ingredients for the inefficient algorithm: performing unitary evolution, and applying the depolarization map on a subset of qubits B (computing the reduced state on the qubits B^c). Unitary evolution follows from $U\rho U^\dagger = \prod_i (1 + U g_i U^\dagger)/2$, and for Clifford unitaries (which preserve the structure Eq. 11), the unitary corresponds to a linear map on the M dimensional subspace. The depolarization of K qubits can also be viewed as a projective linear map which maps the M dimensional subspace of a $2N$ dimensional vector space to a $M' \leq M$ dimensional subspace of a $2(N - K)$ dimensional vector space.

These linear maps can be implemented efficiently by careful consideration of the $2K$ dimensional subspace describing the support of the generators g_i on the K qubits. For example, a unitary action on only K qubits can be implemented by a linear transformation on the $2K$ dimensional subspace. Depolarization of $K < N$ qubits is less efficient and is performed in the following two steps []:

- gaussian elimination
- discarding generators with support on the depolarized qubits
- discarding the trivial support of the remaining generators on the depolarized qubits

The second and third steps are trivial, while the first step corresponds to a change of basis of the M dimensional subspace, $\vec{v}_i \rightarrow \tilde{\vec{v}}_i$, such that

1. only $N_p \leq 2K$ transformed vectors, $\tilde{\vec{v}}_i$, have nonzero projection, $P_K \tilde{\vec{v}}_i \neq 0$ to the $2K$ dimension subspace describing support on the K qubits.
2. the N_p vectors have linearly independent projections on to the $2K$ dimensional subspace.

The second step discards the N_p vectors, and the third step applies the projection $1 - P_K$ to the remaining vectors. Afterwards the reduced state is represented as a $M' = M - N_p$ dimensional subspace of a $2(N - K)$ dimensional vector space. With these two linear maps, the dynamics of the system coupled to the apparatus and environment can be simulated with $O(L^4)$ memory complexity.

B. The efficient algorithm

An efficient algorithm is constructed by realizing the unitary dynamics on the apparatus qubits are trivial after they have coupled to the system. This means the state of an apparatus qubit does not effect the system after it has coupled, and the remaining unitary dynamics can be computed without knowing the support of g_i on the apparatus. Similarly, the depolarization process only requires knowing the projections of v_i on the qubits being depolarized. The main difference with a unitary operation, is the gaussian elimination $\vec{v}_i \rightarrow \tilde{\vec{v}}_i$ effects the projection of the vectors onto the apparatus subspace. Still, one does not need to tract this effect because it has no later effect on projection of the vectors within the system subspace. Finally, computing the entropy of a reduced state only requires knowing the dimensionality of the stabilizer subspace and not the specific form of it. Thus, we can compute the dynamics of the entropies $S(P_S, P'_S; \mathcal{A})$ without tracking the support of the generators on the apparatus qubits that have already coupled to the system. The main limitation of doing so is that we can not compute observables with support on the apparatus or entropies $S(P_S, P'_S; M)$ where $M \neq \mathcal{A}$.

Furthermore, since the apparatus qubits that have not yet coupled to the system are in a trivial product state, we need not keep track of their state explicitly. We therefore only introduce them at the time they interact with the system. Explicitly, at the beginning of the dynamics, a stabilizer pure state is initialized on $S \cup S'$ described by a $4L$ dimension subspace of a $8L$ dimension vector space on \mathcal{F}_2 . As a reminder, each system site contains 2 qubits, such that S and S' contain $4L$ qubits. Numerically, we initialize the state with two completely mixed auxiliary qubits which we use to compute the effect of noisy transduction. As the dynamics evolve, unitary gates transform the support of \vec{v}_i on the system, which we track explicitly.

We perform noisy transduction as follows. First, we initialize the two auxiliary qubits in the initial state of the environment and apparatus. In Hilbert space this looks like

$$\rho \rightarrow \rho \otimes \rho_a \otimes \rho_e = \prod_{i=1}^M \frac{(1 + g_i)}{2} \frac{(1 + g_a)(1 + g_e)}{4} \quad (12)$$

if states ρ_a and ρ_e are initially pure, and

$$\rho \rightarrow \rho \otimes \rho_a \otimes \rho_e = \prod_{i=1}^M \frac{(1+g_i)}{2} \quad (13)$$

if they are maximally mixed. Numerically, additional vector \vec{v}_a and \vec{v}_e representing g_a and g_e are added to the stabilizer subspace for the pure state, while nothing is done for a maximally mixed qubit. The swap gates are then applied, and the auxiliary qubit representing the environment qubit is depolarized, but by skipping step 3 to keep the axially qubit in a maximally mixed state for future use. Then, since we are neglecting the support on the apparatus, the vectors \vec{v}_i are projected to the system subspace, trivializing their support on the auxiliary qubits.

Without any further steps, the number of generators still grows in time as the apparatus qubits are added to the state. This means, the memory complexity would grow as $O(L^2T)$ as we track the support of $O(LT)$ vectors on a $O(L)$ dimensional subspace. This again is inefficient as we do not gain anything by tracking the structure of the linearly dependent sets of vectors. Therefore after each step in the brickwork, we apply gaussian elimination on the $S \cup S'$ subspaces. This will result in a set of vectors having trivial support on the system. We do not need to keep track of these vectors explicitly as they transform trivially under unitary and depolarization channels on the system qubits. Still we cannot ignore them completely since they must have nontrivial support on the apparatus and contribute to the dimensionality of the stabilizer subspace. Thus, in addition to the nontrivial vectors, we keep track of the number of trivial vectors we ignore after this gaussian elimination. Due to this procedure, we only need to keep track the number of ignored vectors, and at most $8L$ vectors describing the non trivial support of the stabilizer subspace on the system. Thus, our memory requirements scale only as $O(L^2)$ allowing for the simulations presented above.

[1] R. Koenig and J. A. Smolin, How to efficiently select an arbitrary clifford group element, *Journal of Mathematical Physics* **55**, 10.1063/1.4903507 (2014).

[2] A. Zabalo, M. J. Gullans, J. H. Wilson, S. Gopalakrishnan, D. A. Huse, and J. H. Pixley, Critical properties of the measurement-induced transition in random quantum circuits, *Phys. Rev. B* **101**, 060301 (2020).

[3] M. J. Gullans and D. A. Huse, Dynamical purification phase transition induced by quantum measurements, *Phys. Rev. X* **10**, 041020 (2020).

[4] Y. Li and M. P. A. Fisher, Statistical mechanics of quantum error correcting codes, *Phys. Rev. B* **103**, 104306 (2021).

[5] R. Fan, S. Vijay, A. Vishwanath, and Y.-Z. You, Self-organized error correction in random unitary circuits with measurement, *Phys. Rev. B* **103**, 174309 (2021).

[6] S. Choi, Y. Bao, X.-L. Qi, and E. Altman, Quantum error correction in scrambling dynamics and measurement-induced phase transition, *Phys. Rev. Lett.* **125**, 030505 (2020).

[7] M. J. Gullans and D. A. Huse, Scalable probes of measurement-induced criticality, *Phys. Rev. Lett.* **125**, 070606 (2020).